ACS APPLIED MATERIALS & INTERFACES

Research Article

www.acsami.org

Novel Quaternized Poly(arylene ether sulfone)/Nano-ZrO_2 Composite Anion Exchange Membranes for Alkaline Fuel Cells

Xiuhua Li,*[,†,‡] Yingfeng Yu,[†,‡] and Yuezhong Meng[§]

[†]School of Chemistry & Chemical Engineering, South China University of Technology, Guangzhou 510641, P.R. China

[‡]The Key Laboratory of Fuel Cell Technology of Guangdong Province, South China University of Technology, Guangzhou 510641, P.R. China

[§]The Key Laboratory of Low Carbon Chemistry & Energy Conservation of Guangdong Province, Sun Yat-Sen University, Guangzhou 510275, P.R. China

ABSTRACT: A series of composite anion exchange membranes based on novel quaternized poly(arylene ether sulfone)/nano-zirconia (QPAES/nano-ZrO_2) composites are prepared using a solution casting method. The QPAES/nano-ZrO_2 composite membranes are characterized by FTIR, X-ray diffraction (XRD), and scanning electron microscopy/energy-dispersive X-ray analysis (SEM/EDX). The ion exchange capacity (IEC), water uptake, swelling ratio, hydroxide ion conductivity, mechanical properties, thermal stability, and chemical stability of the composite membranes are measured to evaluate their applicability in fuel cells. The introduction of nano-ZrO_2 induces the crystallization of the matrix and enhances the IEC of the composite membranes. The modification with nano-ZrO_2 improves water uptake, dimension stability, hydroxide ion conductivity, mechanical properties, and thermal and chemical stabilities of the composite membranes. The QPAES/nano-ZrO_2 composite membranes show hydroxide ion conductivities over 25.7 mS cm^{-1} at a temperature above 60 °C. Especially, the QPAES/nano-ZrO_2 composite membranes with the nano-ZrO_2 content above 7.5% display hydroxide ion conductivities over 41.4 mS cm^{-1} at 80 °C. The E_a values of the QPAES/nano-ZrO2 composite membranes with the nano-ZrO_2 content above 5% are lower than 11.05 kJ mol^{-1}. The QPAES/7.5% nano-ZrO_2 composite membrane displays the lowest E_a value and the best comprehensive properties and constitutes a good potential candidate for alkaline fuel cells.

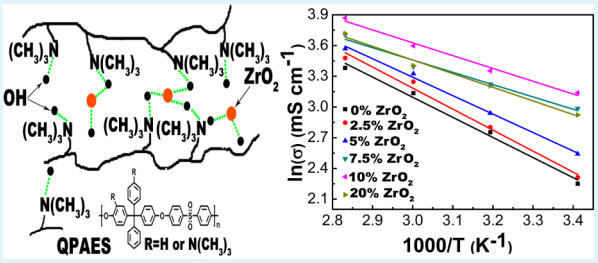

KEYWORDS: *quaternized poly(arylene ether sulfone), nanozirconia, composite membrane, anion exchange membrane, alkaline fuel cells*

1. INTRODUCTION

Fuel cells have been recognized as promising electric energy generators that could provide clean and efficient energy for stationary applications, transportation, and portable power applications since the late 20th century.[1−3] Among the several types of fuel cells, proton exchange membrane fuel cells (PEMFCs) have been highly developed owing to the contribution of perfluorinated acid polymers (e.g., Nafion) with high proton conductivity, good mechanical properties, and excellent stability.[4] Despite the great success, technical issues still exist limiting its widespread commercial applications, which include the high costs of Nafion and noble metal catalysts, slow electrode kinetics, and CO poisoning to noble metal catalysts at low temperatures. Anion exchange membrane fuel cells (AEMFCs) have attracted a lot of attention due to their several potential advantages over PEMFCs, including better electrode reaction kinetics, more options to use nonprecious metals such as Co and Ni as electrocatalysts, and low fuel permeability.[5−8] The development of anion exchange membrane fuels will drastically enhance fuel cell performance and reduce the cost of fuel cells.

As a key component of AEMFCs, anion exchange membranes (AEMs) with good hydroxide ion conductivity, mechanical properties, thermal stability, and chemical stability are desirable, and many efforts have been devoted to develop new AEM materials. A variety of AEMs based on poly(ether ketone)s,[9,10] poly(ether imide)s,[11] poly(phenylene oxide),[12] polystyrene(ethylene butylene)s,[13] poly(phthalazion ether sulfone ketons)s,[14] and poly(arylene ether)s[15−20] have been extensively investigated. Among them, poly(arylene ether)s, a class of aromatic polymers demonstrating excellent thermal and chemical stability, good solubility in organic solvents, and outstanding membrane characteristics, are promising materials for AEMs. In our previous work, a series of AEMs derived from poly(arylene ether)s containing quaternary ammonium groups functionalized tetraphenyl methane moieties demonstrated high hydroxide ion conductivity (20 mS cm^{-1} at 20 °C and 75 mS cm^{-1} at 80 °C, respectively) and good chemical and thermal stabilities. The high hydroxide ion conductivity was

Received: November 26, 2012
Accepted: February 5, 2013
Published: February 5, 2013

attributed to the tetraphenyl methane moieties, which can be loaded up to four ionic groups per unit to give high ion-exchange capacity (IEC).[21] In the cases of polymeric AEMs, the balance between the membrane dimension stability and hydroxide ion conductivity must be taken into full consideration. Recently, organic−inorganic composite materials have been gaining increasing attention for many applications in various fields. They combine the remarkable functionality of organic materials and the stability of inorganic materials.[22,23] In the AEMFC field, several kinds of inorganic fillers such as TiO_2,[24,25] SiO_2,[26,27] α-Al_2O_3,[28] Bentonite,[29] and ZrO_2[30] are being used to modify the AEMs. The addition of an inorganic component enhanced the performance of the AEMs. ZrO_2 is used due to its good physical (hydrophilic) and chemical (inert) properties. ZrO_2 is usually in the form of nanosized particles, which has a high specific surface area, activity, and excellent chemical stability. The introduction of hydrophilic nanosized ZrO_2 fillers results in the reduction of crystallinity and the increase of amorphous phases of the quaternized polymer matrix, leading to an increase of hydroxide ion conductivity of the AEMs. The dimensional stability, mechanical properties, and thermal stability of the nanosized ZrO_2 composite membranes have been greatly enhanced simultaneously.[24,31]

In this work, we attempted to disperse the inorganic nanosized ZrO_2 fillers into the novel quaternized poly(arylene ether sulfone) (QPAES) matrix containing quaternary ammonium groups functionalized tetraphenyl methane moieties, which act as a functional filler capable of enhancing the chemical, thermal, and mechanical properties for the QPAES/nano-ZrO_2 composite membranes. The composite membranes are characterized by FTIR, X-ray diffraction (XRD), scanning electron microscopy/energy-dispersive X-ray analysis (SEM/EDX), and thermogravimetric analysis (TGA). Water uptake, swelling ratio, hydroxide ion conductivity, mechanical properties, and chemical stability of the membranes are evaluated for potential application in AEMFCs.

2. EXPERIMENTAL SECTION

2.1. Materials. Nano-zirconia filler (nano-ZrO_2), 1,1,2,2-tetrachloroethane, 33 wt % trimethylamine solution, and sodium hydroxide were used as purchased. The chloromethylated poly(arylene ether sulfone) (CMPAES) with 1.03 chloromethyl groups per repeating unit and $\bar{M}_n$ = 77 700 Da was prepared according to our previous reported work.[21]

2.2. Preparation of QPAES/Nano-ZrO_2 Composite Membranes. CMPAES was dissolved in 1,1,2,2-tetrachloroethane to form a 5 wt % solution, and the required amount of nano-ZrO_2 was added to the solution and subjected to ultrasonication for about 3 h. The mixture was cast onto a clean glass plate to obtain a composite membrane. The obtained composite membrane was dried at 80 °C for 24 h, and then the membrane was immersed in 33 wt % trimethylamine solution at room temperature for 48 h to be quaternized. After that, the membrane was washed with deionized water three times. Then the membrane was immersed in a 1 M sodium hydroxide aqueous solution at room temperature for 48 h to convert the counteranion from chloride to hydroxide anion. Finally, the membrane was washed with deionized water three times and soaked in deionized water in a closed vessel at least 24 h before analysis. By changing the mass ratios of nano-ZrO_2 to CMPAES, different QPAES/nano-ZrO_2 composite membranes with 2.5, 5, 7.5, 10, and 20 wt % of nano-ZrO_2 were prepared.

2.3. Characterization. The crystal structures of the composite membranes were examined at room temperature by an X-ray diffractometer (D8 ADVANCE, Bruker, Germany) using Cu Kα radiation with a step size of 0.02°, a scan speed of 0.1° s^{-1}, and 2θ angles between 5° and 60°. The crystallinity of the QPAES/nano-ZrO_2 composite membranes was calculated by JADE 6.0.

The composite membrane morphologies were investigated by SEM using a Hitachi S-3700N FESEM with an accelerating voltage of 10 kV. Energy-dispersive X-ray (EDX) spectra of the composite membranes were obtained with the Hitachi S-3700N FESEM.

Mechanical properties of the composite membranes were measured with SANS power testing machine at room temperature and 100% RH at a stretching speed of 50 mm min^{-1}.

Thermogravimetric analysis (TGA) was carried out using a TAINC SDT Q600 thermogravimetric analyzer at a heating rate of 10 °C per minute from 30 to 700 °C under nitrogen atmosphere.

2.3.1. Ion Exchange Capacity (IEC). The IEC of the composite membrane was measured by titration. The dried composite membrane was immersed into 50 mL of standardized HCl (0.01 M) for 24 h, and then a standardized NaOH (0.01 M) solution was used to titrate the HCl solution using phenolphthalein as an indicator. The IEC value is given by

$$\mathrm{IEC} = \frac{(M_1V_1 - M_2V_2)}{W_{\mathrm{dry}}}$$

where M_1 (M) and V_1 (mL) are the concentration and volume of the initial HCl solution. M_2 (M) and V_2 (mL) are the concentration and volume of the standardized NaOH solution used in titration. W_{dry} (g) is the weight of the dry composite membrane.

2.3.2. Water Uptake (WU) and Swelling Ratio (SR). The QPAES/nano-ZrO_2 composite membranes were dried in an oven at 80 °C for 24 h to get a constant weight. The water uptake was measured by immersing the dry membrane into deionized water at a given temperature for 24 h. Then the composite membrane was taken out, and water was wiped away from the surface, and weighted quickly. Water uptake was calculated by

$$\mathrm{WU}\ (\%) = \frac{(W_{\mathrm{wet}} - W_{\mathrm{dry}})}{W_{\mathrm{dry}}} \times 100\%$$

where W_{wet} is the weight of the wet composite membrane and W_{dry} is the weight of the dry membrane.

The swelling ratio (SR) of the composite membranes was measured in the plane direction, which was calculated according to

$$\mathrm{SR} = \frac{(L_{\mathrm{wet}} - L_{\mathrm{dry}})}{L_{\mathrm{dry}}} \times 100\%$$

where L_{wet} was the length of the wet sample in deionized water at a given temperature for 24 h and L_{dry} was the length of the dry membrane.

2.3.3. Hydroxide Ion Conductivity. Hydroxide ion conductivity was measured via the electrochemical impedance spectroscopy (EIS) test with a Solartron 1255B and 1287 frequency response analyzer at an oscillating voltage of 10 mV. The impedance spectra ranged from 1 MHz to 1 kHz. The hydroxide ion conductivity measurement was taken using the two-probe method. Before the test, the QPAE membrane was hydrated in degassed deionized water at least for 24 h. Hydroxide conductivity was calculated using the equation

$$\sigma = \frac{L}{AR}$$

where L (cm) and A (cm^2) are the membrane thickness and the electrode area, respectively, and $R(\Omega)$ is the AC impedance of the membrane.

2.3.4. Chemical Stability Test. The QPAES/nano-ZrO_2 composite membranes were immersed separately into the varying concentrations of NaOH solutions between 1 and 8 M at room temperature for 24 h and then washed thoroughly with deionized water to remove the surface NaOH completely. The hydroxide ion conductivity was measured at 60 °C to study the effect of the cruel alkaline circumstances.

The long-term chemical stability of the QPAES/nano-ZrO_2 composite membranes was further investigated by immersing the samples in 1 M NaOH solution at 60 °C for 240 h. During the testing, we measured the hydroxide ion conductivity at 60 °C and tensile strength at room temperature and took the weight after a certain time.

3. RESULTS AND DISCUSSION

3.1. Structure Characteristic of the QPAES/Nano-ZrO_2 Composite Membranes. The QPAE/10% nano-ZrO_2 composite membrane was characterized by energy-dispersive X-ray (EDX) spectra accompanied with scanning electron microscopy (SEM). The EDX spectrum is shown as Figure 1,

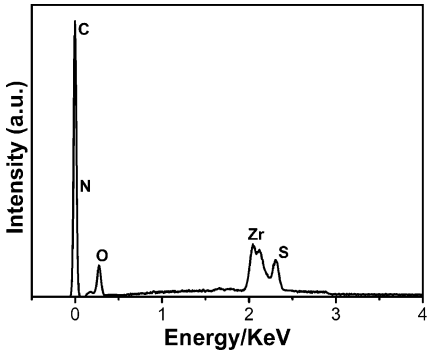

Figure 1. EDX spectrum of the QPAES/10% nano-ZrO_2 composite membrane.

and the corresponding element mapping results are listed in Table 1. It is well-known to the professionals that the EDX can

Table 1. Results of Element Mapping of the QPAES/10% Nano-ZrO_2 Composite Membrane by EDX

element	C	O	S	N	Zr
wt %[a]	32.53	31.85	4.87	10.31	20.44
atom %[a]	49.62	33.90	3.07	4.99	8.42
wt %[b]	67.37	13.54	4.38	1.92	7.40

[a]Determined by EDX. [b]Calculated from the composition of the composite.

determine the mass concentration of the elements with atom numbers over 5 quickly and conveniently. The QPAE/10% nano-ZrO_2 composite contains five kinds of elements (C, N, O, Zr, S), indicating that the chloromethylated poly(arylene ether sulfone) inside the surface layers of the composite membrane was completely converted to quaternized poly(arylene ether sulfone), and nano-ZrO_2 was embedded into the membranes. The calculated mass concentrations of the elements in the QPAES/10% nano-ZrO_2 composite based on the components are listed in Table 1 to help analyze the structure of the composite membrane. The determined mass concentrations of the elements with strong electronegativity are much higher than the calculated values. The reason is the strong coordination between the strong electronegativity element atoms and weak electronegativity element Zr atoms. The strong coordination includes interactions among the quaternary ammonium cations and the counterion hydroxide ions inside the matrix QPAES and interfacial hydrogen bonds between the counterion hydroxide ions and the surface hydroxyl groups of the nano-ZrO_2 particles. Figure 2 shows the schematic diagram of the structure of the poly(arylene ether sulfone)/nano-ZrO_2 composite membrane.

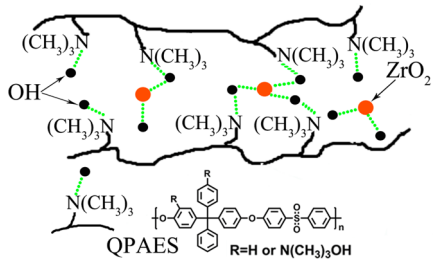

Figure 2. Schematic diagram of the structure of the poly(arylene ether sulfone)/nano-ZrO_2 composite membrane.

The chemical structures of the composite membranes were further investigated by FTIR. The FTIR spectra of the CMPAES, CMPAES/10% nano-ZrO_2, and QPAES/10% nano-ZrO_2 composite membranes are shown in Figure 3,

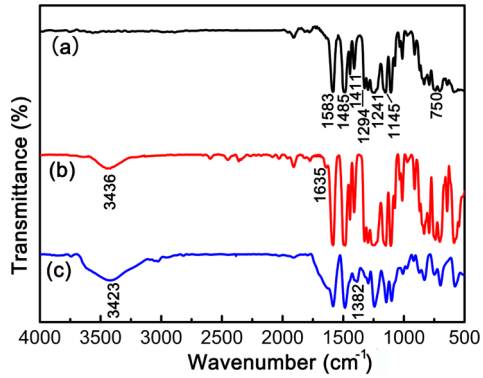

Figure 3. FTIR spectra of the (a) CMPAES, (b) CMPAES/10% nano-ZrO_2, and (c) QPAES/10% nano-ZrO_2 composite membranes.

respectively. The characteristic absorption peaks at 1583 and 1411 cm^{-1} are contributed by the skeletal vibration of the aromatic rings. The sharp peak at 1485 cm^{-1} is assigned to $-CH_2-$. The wide peak around 1241 cm^{-1} is contributed by asymmetric vibration of the ether linkages. The sharp peaks at 1294 and 1145 cm^{-1} are from the asymmetric and symmetric stretching vibration of the O═S═O bonds. The above-mentioned characteristic absorption peaks are attributed to the polymer matrix backbone and appear in all FTIR spectra. The absorption band at 750 cm^{-1} in Figure 3(a) and (b) is assigned to the C−Cl stretch. A new absorption band around 3436 cm^{-1} appears in the spectrum of the CMPAES/10% nano-ZrO_2 composite membrane (Figure 3(b)) compared with the spectrum of the CMPAES membrane (Figure 3(a)). The new absorption band is contributed by −OH groups attached to nano-ZrO_2 particles because of the hygroscopic nature of nano-ZrO_2 particles. The peak at 1635 cm^{-1} originates from the Zr−O−Zr. Compared with the FTIR spectrum of the CMPAES/10% nano-ZrO_2 composite membrane (Figure 3(b)), the absorption band around 3423 cm^{-1} in the spectrum of the QPAES/10% nano-ZrO_2 composite membrane (Figure 3(c)) is enhanced due to the introduction of quaternary ammonium hydroxide and absorbed water. The typical absorption peak of $N-CH_3$ is around 1382 cm^{-1}. The absorption band at 750 cm^{-1} assigned to the C−Cl stretch in Figure 3(c) is weaker than that of Figure 3(a) and 3(b). The remaining signal of the C−Cl stretch in the IR spectrum of the QPAES/nano-ZrO_2 composite membrane reveals the incomplete conversion of chloride to hydroxide anion. The reasonable explanation is that

the quaternization process was carried out in a solid membrane rather than in solutions, and chloromethyl groups inside of the membrane can hardly contact with trimethylamine and result in incomplete functionalization. The combination of FTIR and EDX determination results reflects the structure of the QPAES/nano-ZrO_2 composite membrane from inside to the surface layer.

The X-ray diffraction was scanned to determine the crystallinity of the QPAES and QPAES/nano-ZrO_2 composite membranes. As shown in Figure 4, the diffractogram of QPAES

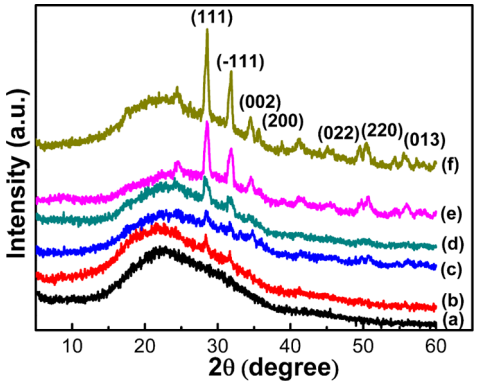

Figure 4. XRD patterns of (a) QPAES, (b) QPAES/2.5% nano-ZrO_2, (c) QPAES/5% nano-ZrO_2, (d) QPAES/7.5% nano-ZrO_2, (e) QPAES/10% nano-ZrO_2, and (f) QPAES/20% nano-ZrO_2.

has no peak and only a halo at 2θ = 13−40° indicating that it is amorphous. There are new sharp peaks appearing in diffractograms of the composite membranes demonstrating the existence of the crystal phase. The intensities of the peaks increase with the increasing loading of nano-ZrO_2. The QPAES/20% nano-ZrO_2 membrane shows the most obvious crystal-phase structure. The sharp peaks appearing at the 2θ angle of 28.60, 31.78, 34.59, 35.58, 49.40, 50.45, and 55.72 are contributed by the nano-ZrO_2 and assigned to (111), (−111), (002), (200), (022), (220), and (013) facets of ZrO_2 crystal, respectively, according to the standard diffractogram of ZrO_2. Compared with a standard diffractogram of ZrO_2, the relative intensities of these peaks in the composite membranes have changed. The crystallinity of the QPAES/nano-ZrO_2 composite membranes calculated by JADE 6.0 is listed in Table 2. The crystallinity of the QPAES/nano-ZrO_2 composite membranes is lower than the crystal filler contents when the nano-ZrO_2 contents in the QPAES/nano-ZrO_2 composites are below 5%. The crystallinity of the QPAES/nano-ZrO_2 composite membranes is higher than the crystal filler contents when the nano-ZrO_2 contents in the QPAES/nano-ZrO_2 composites are over 7.5%, indicating the existence of a new crystal structure. The reasonable explanation is that the strong coordination between the function groups of the matrix QPAES and the nano-ZrO_2 particles induces the crystallization of the QPAES surrounding the nano-ZrO_2 particles. The nucleating effect of nano-ZrO_2 depends greatly on the effective surface area of the nano-ZrO_2 particles. The effective specific surfaces of the nano-ZrO_2 particles in the QPAES/nano-ZrO_2 composites decrease with the increasing loading of the nano-ZrO_2 owing to the formation of agglomerates. This conduction agrees well with the observations in the SEM photographs (Figure 5). The XRD testing results of the QPAES/nano-ZrO_2 composites are contrary to the reported nano-ZrO_2 composite AEMs.[24,31,32]

3.2. Morphology. The surface morphology of the QPAES/nano-ZrO_2 composite membranes is characterized and shown in Figure 5 as SEM photographs at a magnification of 5000×. The surface of the QPAES/2.5% nano-ZrO_2 composite membrane (Figure 5(a)) indicates uniform distribution of the nano-ZrO_2 fillers and excellent compatibility between the polymer matrix and inorganic phase. In Figure 5(b) and 5(c), the SEM images of the QPAES/nano-ZrO_2 composites with filler contents of 5% and 7.5%, respectively, the filler particles can be observed evenly distributed with a negligible amount of agglomeration on the surfaces of the membranes. When the content of nano-ZrO_2 is above 10%, the agglomeration of nano-ZrO_2 fillers is enhanced with the increasing nanofiller loading, and the sizes of the ZrO_2 agglomerates or chunks distribute randomly around 20−30 μm (Figure 5(d) and 5(e)). However, there are no cracks between the matrix and the filler agglomerates. This implies that the prepared composite membranes can be expected to perform consistently well in the AEMFCs.

3.3. Ion Exchange Capacity (IEC), Water Uptake, Swelling Ratio, Hydroxide Ion Conductivity, and Mechanical Properties. The IEC values, water uptakes, swelling ratios, hydroxide conductivities, and mechanical properties are the basic performance parameters for AEMs. The dependence of the IEC value on the nano-ZrO_2 loading is investigated and listed in Table 2. The experimental IEC value of the QPAES membrane is lower than the theoretical IEC value calculated from the chloromethyl group density of CMPAE based on the assumption of complete quaternization and alkalization. The reasonable explanations for the disparity include incomplete functionalization inside the membrane and the competing side reaction of benzyl chloride to benzyl alcohol during the quaternization. The experimental IEC values of the QPAES/nano-ZrO_2 composite membranes are higher than the theoretical IEC values calculated from the loading ratios of CMPAE and the chloromethyl group density of CMPAE. The testing results strongly support the conductions from the EDX, XRD, and SEM. The good mixing and strong coordination between the matrix and the nano-ZrO_2 particles increase the effective surfaces of the nanofillers coordinating

Table 2. Crystallinity and IEC Values of the QPAES/Nano-ZrO_2 Composite Membranes

membrane	crystallinity (%)	IEC[a] (meq g^{-1})	IEC[b] (meq g^{-1})	IEC of ZrO_2 (meq g^{-1})	IEC of 1% ZrO_2
QPAES	0	1.57	1.46 ± 0.21	0	0
QPAES/2.5% ZrO_2	2.09	1.53	1.58 ± 0.15	0.16	0.064
QPAES/5% ZrO_2	3.89	1.49	1.61 ± 0.17	0.22	0.044
QPAES/7.5% ZrO_2	9.29	1.45	1.74 ± 0.03	0.39	0.052
QPAES/10% ZrO_2	10.42	1.41	1.82 ± 0.37	0.51	0.051
QPAES/20% ZrO_2	23.11	1.25	1.70 ± 0.09	0.53	0.027

[a]Calculated from DCM and the compositions of the composite membranes. [b]Determined by titration.

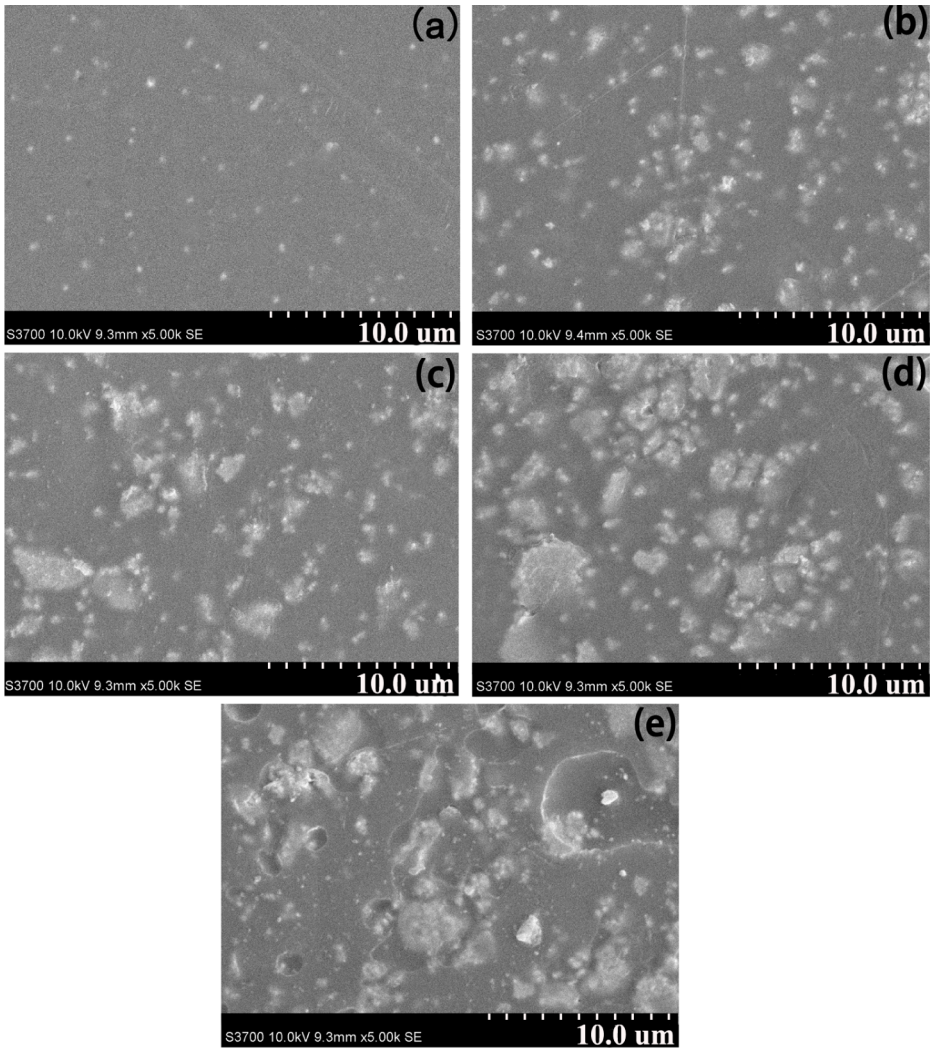

Figure 5. SEM images of (a) QPAES/2.5% nano-ZrO_2, (b) QPAES/5% nano-ZrO_2, (c) QPAES/7.5% nano-ZrO_2, (d) QPAES/10% nano-ZrO_2, and (e) QPAES/20% nano-ZrO_2.

Table 3. Water Uptake, Swelling Ratio, and Hydroxide Ion Conductivity of the QPAES and QPAES/Nano-ZrO_2 Composite Membranes

		water uptake (%)		swelling ratio (%)	conductivity (mS cm^{-1})	
membrane	IEC (meq g^{-1})	20 °C	60 °C	60 °C	20 °C	60 °C
QPAES	1.46 ± 0.21	10.3	33.2	11.4	9.5 ± 0.6	21.6 ± 0.9
QPAES/2.5% nano-ZrO_2	1.58 ± 0.15	12.1	35.9	11.3	10.1 ± 0.7	25.7 ± 1.4
QPAES/5% nano-ZrO_2	1.61 ± 0.17	15.6	40.3	9.8	12.7 ± 1.5	27.8 ± 0.3
QPAES/7.5% nano-ZrO_2	1.74 ± 0.03	23.8	52.7	8.6	19.8 ± 0.8	30.4 ± 1.2
QPAES/10% nano-ZrO_2	1.82 ± 0.37	28.1	63.9	7.4	23.1 ± 2.1	36.5 ± 0.6
QPAES/20% nano-ZrO_2	1.70 ± 0.09	25.7	60.4	7.5	18.6 ± 1.6	30.1 ± 1.2

more hydroxide ion to give high IEC values. The contribution of the nanofillers to IEC values of the QPAES/nano-ZrO_2 composite membranes varies with the nanofiller loading. The parameter IEC of 1% ZrO_2 in Table 2 reflects the contribution ability of IEC at the different nanofiller loadings. The contribution ability of IEC shows a decreasing trend with the increasing content of nano-ZrO_2. The contribution ability of IEC is weakened greatly at the maximum loading owing to the obvious agglomeration of nano-ZrO_2 fillers. The cumulative contribution of the nano-ZrO_2 fillers displays the fact that the experimental IEC values of the QPAES/nano-ZrO_2 composite membranes demonstrate the enhanced values ranging from 1.46 to 1.82 meq g^{-1}.

The water uptake, swelling ratio, and hydroxide conductivity of the QPAES and QPAES/nano-ZrO_2 composite membranes are listed in Table 3. The water uptake values of QPAES and QPAES/composite membranes increase with the increasing IEC. The membranes exhibit higher water uptake abilities at higher temperature. Meanwhile, the presence of nano-ZrO_2 enhances the ability of water absorption of QPAES/nano-ZrO_2 composite membranes. The water uptakes increase with increasing nano-ZrO_2 content until the nano-ZrO_2 content up to 10%. This is due to the hygroscopic and water retention

nature of nano-ZrO_2 particles. The water uptakes of the QPAES/nano-ZrO_2 composite membranes with nano-ZrO_2 content over 10% show the decreasing tendency. The reasonable explanation is that the self-glomeration of the nano-ZrO_2 particles is enhanced with the additional amount of nano-ZrO_2 particles after a threshold nano-ZrO_2 content, and the density of hydroxyl groups attached onto the surface of nano-ZrO_2 aggregates decreases with the increasing size of nano-ZrO_2 aggregates. The swelling ratios of the QPAES/nano-ZrO_2 composite membranes were effectively reduced with the addition of nano-ZrO_2 compared with virgin QPAES. The dimension stabilities of the QPAES/nano-ZrO_2 composite membranes were effectively enhanced by the introduction of nano-ZrO_2 fillers.

The temperature and IEC dependences of hydroxide ion conductivities of the QPAES and QPAES/nano-ZrO_2 composite membranes are also recorded in Table 3 and Figure 6. The

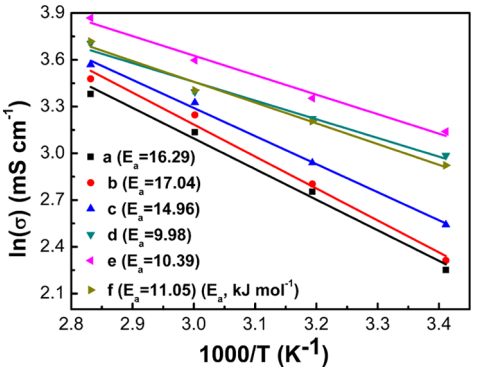

Figure 6. Temperature dependence of hydroxide ion conductivities of the QPAES and QPAES/nano-ZrO_2 composite membranes ((a) QPAES, (b) QPAES/2.5% nano-ZrO_2, (c) QPAES/5% nano-ZrO_2, (d) QPAES/7.5% nano-ZrO_2, (e) QPAES/10% nano-ZrO_2, and (f) QPAES/20% nano-ZrO_2).

dependences of hydroxide ion conductivity on IEC and temperature is similar to that of water uptakes. The hydroxide ion conductivities of the QPAES/nano-ZrO_2 composite membranes increase with the increasing temperature. The hydroxide ion conductivities of the QPAES/nano-ZrO_2 composite membranes are enhanced significantly owning to the enhanced IECs with the increasing loading of nano-ZrO_2 filler. The enhancing trend in hydroxide ion conductivities agrees well with the increasing trend in the crystallinity of the QPAES/nano-ZrO_2 composite membranes. The fact enlightens us that the crystal phase may facilitate the establishment of the hydroxide ion conductive channels in the hydrated membranes owing to the fix of the functional groups inside the crystal phase. The QPAES/nano-ZrO_2 composite membranes exhibit hydroxide ion conductivities in the ranges of 10.1−23.1 mS cm^{-1} at 20 °C, 25.7−36.5 mS cm^{-1} at 60 °C, and 32.4−47.9 mS cm^{-1} at 80 °C, respectively. Especially, the QPAES/nano-ZrO_2 composite membranes with the nano-ZrO_2 content above 7.5% display hydroxide ion conductivities above 41.4 mS cm^{-1} 80 °C. All the QPAES/nano-ZrO_2 composite membranes show hydroxide ion conductivities over 25.7 mS cm^{-1} at temperature above 60 °C, which can satisfy the requirement of AEMs used in AEMFCs. The QPAES/10% nano-ZrO_2 composite membrane demonstrates the highest hydroxide ion conductivity (47.9 mS cm^{-1}) at 80 °C, which is almost 1.4 times higher than that of the virgin QPAES membrane (29.4 mS cm^{-1}). This can be explained by the inherent ion transport activation energies (E_a) of the various QPAES/nano-ZrO_2 composite membranes and the IEC values determined by titration.

The E_a values were calculated according to the equation: $E_a = -b \times R$, where b is the slope of the regressed linear ln $\sigma \sim 1000/T$ plot, and R is the gas constant (8.314 J (mol K)$^{-1}$). The E_a values of the QPAES/nano-ZrO_2 composite membranes decrease with the increasing content of nano-ZrO_2 until nano-ZrO_2 content arrives at 7.5% (Figure 6). The QPAES/7.5% nano-ZrO_2 composite membrane has the lowest E_a (9.98 kJ mol^{-1}). Then, the E_a values of the QPAES/nano-ZrO_2 composite membranes demonstrate a slow increase with the increasing nano-ZrO_2 content. All the E_a values of the QPAES/nano-ZrO_2 composite membranes with the nano-ZrO_2 content above 5% are lower than that of Nafion-117 (12.75 kJ mol^{-1})[33] and some organic−inorganic composite membranes.[34,35] The reason for the E_a jump of QPAES/nano-ZrO_2 composite membranes at a nano-ZrO_2 content of 7.5% is the ionic groups of QPAES and nano-ZrO_2 filler which both transport the hydroxide ion in the hydrated composite membranes. When the nano-ZrO_2 content is below 7.5%, the nano-ZrO_2 particles are isolated by the QPAES matrix, and the conductivity depends mainly on the QPAES matrix. The E_a values of the QPAES/nano-ZrO_2 composite membranes with the nano-ZrO_2 content below 7.5% are close to that of the QPAES (16.29 kJ mol^{-1}). When the nano-ZrO_2 content is up to 7.5%, the effective hydroxide ion transport channels have been established from the continuous hydroxide ion conductive phase. The crystal QPAES phase surrounding the hygroscopic nano-ZrO_2 particles facilitates the formation of the continuous hydroxide ion conductive phase in the hydrated membranes owing to the crystal phase originating from the segments rich in hygroscopic functional groups. The enhanced self-glomeration of the nano-ZrO_2 particles with the increasing nano-ZrO_2 loading increases the size of nano-ZrO_2 aggregates and decreases the nucleating effect of nano-ZrO_2 and the density of hydroxyl groups attached onto the surface of nano-ZrO_2 aggregates and thus enhances slightly the temperature dependence of hydroxide ion conductivities of the QPAES/nano-ZrO_2 composite membranes with the nano-ZrO_2 content above 7.5%.

The mechanical properties of the QPAES and QPAES/nano-ZrO_2 composite membranes were measured at room temperature and 100% RH. As shown in Figure 7, tensile strength and percentage elongation of the QPAES/nano-ZrO_2 composite membranes are strengthened with the introduction of nano-ZrO_2 fillers. The enhancement of mechanical properties results from the strong interactions between the polymer matrix and

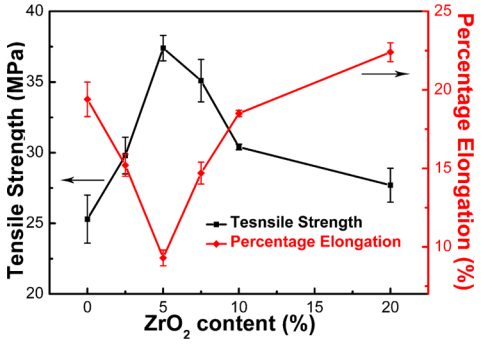

Figure 7. Variation of tensile strength and percentage elongation with the addition of nano-ZrO_2.

dx.doi.org/10.1021/am302844x | ACS Appl. Mater. Interfaces 2013, 5, 1414−1422

the inorganic filler phase. The reinforcement varies with the additional contents of nano-ZrO_2. The optimum reinforcement is obtained with the nano-ZrO_2 content of 5.0%. The QPAES/5% nano-ZrO_2 composite membrane gives a maximum tensile strength up to 37.4 MPa. The decrease in tensile strength at the nano-ZrO_2 content above 5% is due to agglomerate formation which would result in initiation of catastrophic failure of the composites under the loading of stress. Even the effect of the nano-ZrO_2 agglomerate is negative; the strong positive interaction between the polymer matrix and the inorganic filler phase reinforces the mechanical properties of the QPAES/nano-ZrO_2 composite at the investigating nano-ZrO_2 contents.

3.4. Thermal Stability and Chemical Stability. The thermal stability and chemical stability are important criteria of AEMs used in fuel cells because some AEMs are usually not stable at AEMFC working conditions such as strong basic circumstance and elevated temperature.[36]

The thermal stability of QPAES and QPAES/nano-ZrO_2 composite membranes was investigated by TGA technique. As shown in Figure 8, the TGA curves of QPAES and QPAES/nano-ZrO_2 composite membranes divide into three main stages. The first stage is from 30 to 170 °C corresponding to the removal of residual water. The second weight loss stage commencing around 170 °C is assigned to the degradation of quaternary ammonium groups. The third weight loss stage at temperature higher than 360 °C is assigned to the polymer backbone decomposition. The degradation trends of the QPAES and QPAES/nano-ZrO_2 composite membranes are almost the same, and the QPAES/nano-ZrO_2 composite membranes are slightly more stable than the QPAES membrane. This may be explained by the addition of inorganic filler of nano-ZrO_2 into the composites. The high thermal stability of nano-ZrO_2 and the interaction between the polymer matrix and the inorganic filler phase increase the thermal stability of the QPAES/nano-ZrO_2 composite membranes. The QPAES/nano-ZrO_2 composite membranes demonstrate acceptable short-term thermal stabilities.

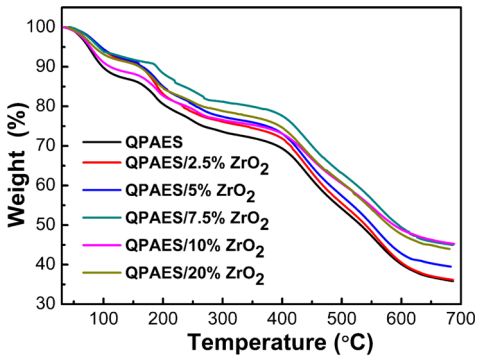

Figure 8. TGA curves for the QPAES and QPAES/nano-ZrO_2 membranes.

The chemical stability of the QPAES and QPAES/nano-ZrO_2 composite membranes was investigated by immersing the membrane samples in 1−8 M NaOH solutions at room temperature. The variations of hydroxide ion conductivity at 60 °C of the testing membranes were characterized. As shown in Figure 9, the QPAES and QPAES/nano-ZrO_2 composite membranes show similar trends in hydroxide ion conductivities along with the concentrations of NaOH. The hydroxide ion conductivities increase with the increasing concentration of NaOH up to a threshold. Then the hydroxide ion conductivities show decreasing tendency after the peak. Under the NaOH concentration of 8 M, the hydroxide ion conductivities of all the treated membranes are lower than the virgin membranes. All the QPAES/nano-ZrO_2 composite membranes exhibit a decrease less than 15.5%, while the QPAES membrane shows a decrease of 17.8%. That means the QPAES/nano-ZrO_2 composite membranes are more stable than the QPAES membrane under a broad strong basic condition.

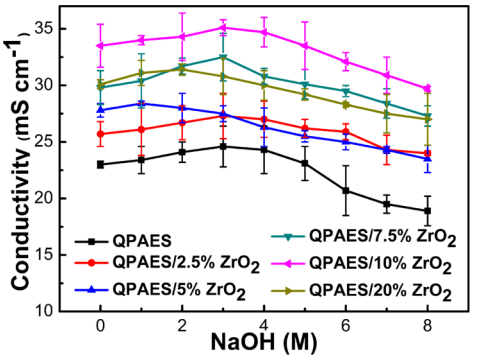

Figure 9. Effect of NaOH concentrations on hydroxide ion conductivity of the QPAES and QPAES/nano-ZrO_2 composite membranes.

The long-term chemical stability of the QPAES and QPAES/nano-ZrO_2 composite membranes was further investigated in terms of weight remaining, hydroxide ion conductivity, and tensile strength in 1 M NaOH at 60 °C. Figure 10 shows the time dependences of the weight remaining of QPAES and QPAES/nano-ZrO_2 composite membranes. Both QPAES and QPAES/nano-ZrO_2 composite membranes display similar trends in the first 72 h. The weights of the membranes increase less than 3%. The initial increase in weight may be because the effect of the swelling of the membranes overwhelms that of the degradation of the membranes. Then the weights of the membranes decrease slowly with the elapsing testing time, which resulted from the decomposition of the ionic groups and polymer backbone. The weight losses of the composite membranes range from 3.0 to 4.9% at a testing time of 240 h. The variations in the hydroxide ion conductivity and tensile strength of the QPAES and QPAES/nano-ZrO_2 composite membranes before and after chemical stability test in 1 M NaOH at 60 °C for 170 h are summarized in Table 4. Compared with the initial conductivity values and tensile

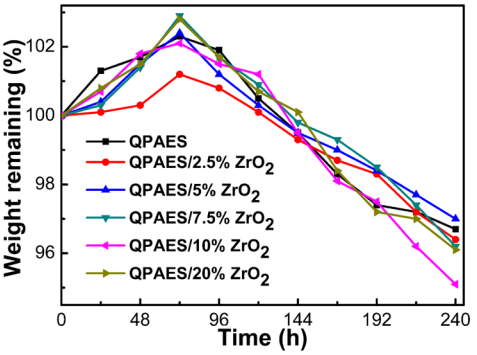

Figure 10. Weight remaining of the QPAES and QPAES/nano-ZrO_2 composite membranes in 1 M NaOH solution at 60 °C.

Table 4. Variation in Hydroxide Ion Conductivity and Tensile Strength of the QPAES and QPAES/Nano-ZrO_2 Composite Membranes after the Stability Test

		stability test condition			decreasing amplitude (%)	
membrane	IEC (meq g^{-1})	concentration	temperature	time	conductivity (60 °C)	tensile strength
QPAES	1.46 ± 0.21	1 M NaOH	60 °C	170 h	11.5	7.5
QPAES/2.5% ZrO_2	1.58 ± 0.15	1 M NaOH	60 °C	170 h	12.3	8.1
QPAES/5% ZrO_2	1.61 ± 0.17	1 M NaOH	60 °C	170 h	11.8	8.9
QPAES/7.5% ZrO_2	1.74 ± 0.03	1 M NaOH	60 °C	170 h	9.3	9.2
QPAES/10% ZrO_2	1.82 ± 0.37	1 M NaOH	60 °C	170 h	13.4	7.4
QPAES/20% ZrO_2	1.70 ± 0.09	1 M NaOH	60 °C	170 h	12.7	10.3
O-PBIMe2731[37]	not reported	1 M KOH	60 °C	24 h	breaks when handled	
QPEK−OH[38]	0.41	1 M KOH	60 °C	120 h	40	not reported

strength values, the testing results showed 9.3%−13.4% decreasing amplitudes of conductivity values and 7.4%−10.3% decreasing amplitudes of tensile strength. And especially the decreasing amplitude of the conductivity of the QPAES/7.5% nano-ZrO_2 composite membrane is smaller than that of the QPAES membrane. The determination results indicate that the QPAES/nano-ZrO_2 composite membranes exhibit more excellent long-term alkaline stability than some reported AEMs.[37,38]

4. CONCLUSIONS

In summary, novel quaternized poly(arylene ether sulfone)/nanozirconia (QPAES/nano-ZrO_2) composite anion exchange membranes are successfully fabricated from poly(arylene ether sulfone) containing quaternary ammonium group functioned tetraphenyl methane moieties and nanosized ZrO_2 filler. SEM images reveal the nano-ZrO_2 particles distribute uniformly with the nano-ZrO_2 content below 10 wt %. EDX results disclose the strong coordination among quaternary ammonium cations, hydroxide ions, and the nano-ZrO_2 particles. XRD spectra reveal that the crystallinity of the QPAES/nano-ZrO_2 composites increases with the increasing nanofiller loading. The strong coordination between the functional groups of the matrix QPAES and the nano-ZrO_2 particles induces the crystallization of the QPAES surrounding the nano-ZrO_2 particles. The crystal QPAES phase surrounding the hygroscopic nano-ZrO_2 particles is useful for the enhancement of hydroxide ion conductivity. The water uptake, dimension stability, hydroxide ion conductivity, mechanical properties, thermal stability, and chemical stability of the QPAES/nano-ZrO_2 composite membranes are enhanced by the introduction of nano-ZrO_2. All the QPAES/nano-ZrO_2 composite membranes show hydroxide ion conductivities over 25.7 mS cm^{-1} at temperature above 60 °C, which can satisfy the requirement of AEMs used in AEMFCs. Especially, the QPAES/nano-ZrO_2 composite membranes with the nano-ZrO_2 content above 7.5% display hydroxide ion conductivities above 41.4 mS cm^{-1} at 80 °C. All the E_a values of the QPAES/nano-ZrO_2 composite membranes with the nano-ZrO_2 content above 5% are below 11.05 kJ mol^{-1}. The QPAES/7.5% nano-ZrO_2 composite membrane displays the lowest E_a value and highest chemical stability. The QPAES/7.5% nano-ZrO_2 composite membrane exhibits the best comprehensive properties and seems promising for application in fuel cells.

AUTHOR INFORMATION

Corresponding Author

*Tel. & Fax: 8620-22236591. E-mail: lixiuhua@scut.edu.cn.

Notes

The authors declare no competing financial interest.

ACKNOWLEDGMENTS

The work was supported by the National Natural Science Foundation of China (NSFC) (Grant 51173045), Research Fund of the Key Laboratory of Low Carbon Chemistry & Energy Conservation of Guangdong Province (Grant 20100103), Research Fund of the Key Laboratory of Fuel Cell Technology of Guangdong Province (Grant 201104), and SRP Fund of South China University of Technology (Grant 20120147).

REFERENCES

(1) Steele, B. C.; Heinzel, A. *Nature* **2001**, *414*, 345−52.
(2) Carrette, L.; Friedrich, K. A.; Stimming, U. *Fuel Cells* **2001**, *1*, 5−39.
(3) Jacobson, M. Z.; Colella, W. G.; Golden, D. M. *Science* **2005**, *308*, 1901−1905.
(4) Mehta, V.; Cooper, J. S. *J. Power Sources* **2003**, *114*, 32−53.
(5) Lu, S.; Pan, J.; Huang, A.; Zhuang, L.; Lu, J. *Proc. Natl. Acad. Sci. U.S.A.* **2008**, *105*, 20611−20614.
(6) Sanabria-Chinchilla, J.; Asazawa, K.; Sakamoto, T.; Yamada, K.; Tanaka, H.; Strasser, P. *J. Am. Chem. Soc.* **2011**, *133*, 5425−5431.
(7) Tanaka, M.; Fukasawa, K.; Nishino, E.; Yamaguchi, S.; Yamada, K.; Tanaka, H.; Bae, B.; Miyatake, K.; Watanabe, M. *J. Am. Chem. Soc.* **2011**, *133*, 10646−10654.
(8) Varcoe, J. R.; Slade, R. C. T.; Lam How Yee, E. *Chem. Commun.* **2006**, 1428−1429.
(9) Zhang, H.; Zhou, Z. *J. Appl. Polym. Sci.* **2008**, *110*, 1756−1762.
(10) Xiong, Y.; Liu, Q. L.; Zeng, Q. H. *J. Power Sources* **2009**, *193*, 541−546.
(11) Wang, G. G.; Weng, Y. M.; Chu, D.; Xie, D.; Chen, R. R. *J. Membr. Sci.* **2009**, *326*, 4−8.
(12) Wu, L.; Zhou, G. F.; Liu, X.; Zhang, Z. H.; Li, C. R.; Xu, T. W. *J. Membr. Sci.* **2011**, *371*, 155−162.
(13) Vinodh, R.; Ilakkiya, A.; Elamathi, S.; Sangeetha, D. *Mater. Sci. Eng., B* **2010**, *167*, 43−50.
(14) Fang, J.; Shen, P. K. *J. Membr. Sci.* **2006**, *285*, 317−322.
(15) Wang, J. H.; Li, S. H.; Zhang, S. B. *Macromolecules* **2010**, *43*, 3890−3896.
(16) Zhao, Z.; Wang, J. H.; Li, S. H.; Zhang, S. B. *J. Power Sources* **2011**, *196*, 4445−4450.
(17) Tanaka, M.; Koike, M.; Miyatake, K.; Watanabe, M. *Macromolecules* **2010**, *43*, 2657−2659.
(18) Tanaka, M.; Koike, M.; Miyatake, K.; Watanabe, M. *Polym. Chem.* **2011**, *2*, 99−106.
(19) Zhang, F. X.; Zhang, H. M.; Qu, C. *J. Mater. Chem.* **2011**, *21*, 12744−12752.
(20) Liu, G. S.; Shang, Y. M.; Xie, X. F.; Wang, S. B.; Wang, J. H.; Wang, Y. W.; Mao, Z. Q. *Int. J. Hydrogen Energy* **2012**, *37*, 848−853.

(21) Li, X.; Yu, Y.; Liu, Q.; Meng, Y. *ACS Appl. Mater. Interfaces* **2012**, *4*, 3627−3635.
(22) Sanchez, C.; Julian, B.; Belleville, P.; Popall, M. *J. Mater. Chem.* **2005**, *15*, 3559−3592.
(23) Kickelbick, G. *Prog. Polym. Sci.* **2003**, *28*, 83−114.
(24) Yang, C. C.; Chiu, S. J.; Lee, K. T.; Chien, W. C.; Lin, C. T.; Huang, C. A. *J. Power Sources* **2008**, *184*, 44−51.
(25) Yang, C. C. *J. Membr. Sci.* **2007**, *288*, 51−60.
(26) Wu, Y. H.; Luo, J. Y.; Yao, L. L.; Wu, C. M.; Mao, F. L.; Xu, T. W. *J. Membr. Sci.* **2012**, *399*, 16−27.
(27) Yang, C. C.; Chiu, S. S.; Kuo, S. C.; Liou, T. H. *J. Power Sources* **2012**, *199*, 37−45.
(28) Mohamad, A. A.; Arof, A. K. *Mater. Lett.* **2007**, *61*, 3096−3099.
(29) Sang, S. B.; Zhang, J. F.; Wu, Q. M.; Liao, Y. G. *Electrochim. Acta.* **2007**, *52*, 7315−7321.
(30) Vinodh, R.; Purushothaman, M.; Sangeetha, D. *Int. J. Hydrogen Energy* **2011**, *36*, 7291−7302.
(31) Yang, C. C.; Li, Y. J.; Chiu, S. J.; Lee, K. T.; Chien, W. C.; Huang, C. A. *J. Power Sources* **2008**, *184*, 95−98.
(32) Wang, E. D.; Zhao, T. S.; Yang, W. W. *Int. J. Hydrogen Energy* **2010**, *35*, 2183−2189.
(33) Lin, B. C.; Qiu, L. H.; Lu, J. M.; Yan, F. *Chem. Mater.* **2010**, *22*, 6718−6725.
(34) Xiong, Y.; Liu, Q. L.; Zhang, Q. G.; Zhu, A. M. *J. Power Sources* **2008**, *183*, 447−453.
(35) Xiong, Y.; Fang, J.; Zeng, Q. H.; Liu, Q. L. *J. Membr. Sci.* **2008**, *311*, 319−325.
(36) Lin, B. C.; Qiu, L. H.; Qiu, B.; Peng, Y.; Yan, F. *Macromolecules* **2011**, *44*, 9642−9649.
(37) Henkensmeier, D.; Cho, H. R.; Kim, H. J.; Kirchner, C. N.; Leppin, J.; Dyck, A.; Jang, J. H.; Cho, E.; Nam, S. W.; Lim, T. H. *Polym. Degrad. Stab.* **2012**, *97*, 264−272.
(38) Zarrin, H.; Wu, J.; Fowler, M.; Chen, Z. W. *J. Membr. Sci.* **2012**, *394*, 193−201.